frontiers in Chemistry

ORIGINAL RESEARCH
published: 07 August 2020
doi: 10.3389/fchem.2020.00639

Ultra-Weak Chemiluminescence Enhanced by Cerium-Doped LaF_3 Nanoparticles: A Potential Nitrite Analysis Method

Yufei Wang[1], *Yanran Wang*[1], *Chunxia Huang*[1], *Tianyou Chen*[1] *and Jing Wu*[1,2]*

[1] School of Science, China University of Geosciences, Beijing, China, [2] Key Laboratory of Optic-electric Sensing and Analytical Chemistry for Life Science, MOE, Qingdao University of Science and Technology, Qingdao, China

In this work, cerium-doped LaF_3 nanoparticles (LaF_3:Ce NPs) were successfully synthesized and characterized. Its chemiluminescence (CL) property was studied, and it was amazingly found that it intensely enhanced the ultra-weak CL of the $NaNO_2$-H_2O_2 system. The CL mechanism was systematically investigated and suggested to be the recombination of electron-injected and hole-injected LaF_3:Ce NPs. The new CL system was developed to be a facile, original, and direct method for nitrite analysis. Experimental conditions were optimized and then a satisfactory linear relationship between CL intensity and nitrite concentration was obtained. This work introduced a new pathway for the research and application of traditional fluoride NPs doped with RE^{3+}.

Keywords: chemiluminescence, cerium, fluoride, nitrite, nanoparticles

OPEN ACCESS

Edited by:
Qianqian Su,
Shanghai University, China

Reviewed by:
Xiaoji Xie,
Nanjing Tech University, China
Suli Wu,
Dalian University of Technology, China

***Correspondence:**
Jing Wu
wujing@cugb.edu.cn

Specialty section:
This article was submitted to Nanoscience, a section of the journal Frontiers in Chemistry

Received: *28 May 2020*
Accepted: *19 June 2020*
Published: *07 August 2020*

Citation:
Wang Y, Wang Y, Huang C, Chen T and Wu J (2020) Ultra-Weak Chemiluminescence Enhanced by Cerium-Doped LaF_3 Nanoparticles: A Potential Nitrite Analysis Method. Front. Chem. 8:639. doi: 10.3389/fchem.2020.00639

INTRODUCTION

Fluoride is utilized as an ideal and appealing host for phosphors doped with rare earth ions (RE^{3+}) owing to its adequate thermal and environmental stability as well as large solubility for RE^{3+} ions (Li et al., 2012). Compared with oxide systems, vibrational energies in fluorides is low and therefore trigger scarce quenching of the excited states of the RE^{3+} ions (Bender et al., 2000). Furthermore, RE^{3+}-doped fluorides exhibit characteristic properties, such as high ionicity, low refractive index, wide band gap, and low phonon energy. $KMgF_3$ (Schuyt and Williams, 2018), $NaYF_4$ (Wu et al., 2019, 2020), $NaGdF_4$ (Yi et al., 2019), and LaF_3 (Bekah et al., 2016; Nampoothiri et al., 2017) have been investigated and exhibit high quantum yields and long luminescent lifetimes. RE^{3+}-doped fluorides have been attracting attentions for several years due to the wide variety of technological applications including biomedical researches (All et al., 2019; Yan et al., 2019), biosensors (Vijayan et al., 2019), bioimaging (Hu et al., 2016; Han et al., 2017; Zeng et al., 2019), radiation detection (Ju et al., 2017), optoelectronic devices (Wu et al., 2018), and so on. However, to the best of our knowledge, the performance of RE^{3+}-doped fluorides toward chemiluminescence (CL) has not been explored.

Nitrite is widely used in food manufacture as preservatives and fertilizing reagents. As an essential precursor of carcinogenic *N*-nitrosamine, excess intake of nitrite is harmful for human beings. Nitrite can cause irreversible conversion of hemoglobin to methemoglobin in the bloodstream and then bring detrimental effect for the oxygen transport in the whole body. In addition, nitrogen-based fertilizers and industrial wastewater pollute groundwater resources by nitrites. Thus, nitrite detection is of significant importance for food safety, public health, and environment protection (Wang et al., 2017; Zhang Y. et al., 2018; Cao et al., 2019).

Various principle-based analytical methods have been devised for nitrite detection, such as electrochemical sensors (Ma et al., 2018; Wang et al., 2018; Zhou et al., 2019; Madhuvilakku et al., 2020), microplasma emission (Zheng et al., 2018), absorption spectrophotometry (Zhang L. et al., 2018), fluorescence (Dai et al., 2017; Jana et al., 2019; Pires et al., 2019), and CL (Lu et al., 2002, 2004; Lin et al., 2011; Wu et al., 2016). Electrodes are modified with complex strategies in electrochemical analysis. Special molecules need to be designed for spectrophotometric detections in order to amplify signal and reduce the background interferences. CL detections require simple instruments, interfere with low background, and are compatible with gas or aqueous phases. CL intensity was reported to be significantly enhanced by nanomaterials that gave promise for developing sensitive and convenient CL analytical methods. In 2011, carbon dots were firstly demonstrated to enhance the CL signal of the $NaNO_2$-H_2O_2 system because of peroxynitrous acid generation (Lin et al., 2011). Nitrogen-rich quantum dots (QDs) were facilely synthesized and intensely enhanced the ultra-weak CL reaction of the $NaIO_4$-H_2O_2 system through electron hole injection and CL resonance energy transfer (Zheng et al., 2017). In particular, molybdenum sulfide QDs were proved to give rise to the generation of reactive oxygen species from hydrogen peroxide (H_2O_2) in alkaline solution and gave a promise for CL emission (Dou et al., 2019). However, fluoride-based nanomaterials were scarcely utilized and the developed CL analysis was rarely applied in nitrite detection. Original CL detections for nitrites are worth giving research to pursue better performance.

In this work, cerium-doped LaF_3 nanoparticles (LaF_3:Ce NPs) were synthesized and firstly demonstrated to enhance the CL signal of the $NaNO_2$-H_2O_2 system. Reactive oxygen species generation that was triggered by LaF_3:Ce NPs was proved to be the main reason for CL enhancement. A linear relationship between the CL signal and nitrite concentration was found and implied that the LaF_3:Ce NPs-$NaNO_2$-H_2O_2 system could be applied in the determination of nitrite.

MATERIALS AND METHODS

Reagents and Materials

Sodium nitrite ($NaNO_2$) was purchased from Sinopharm Chemical Reagent Co., Ltd. (Shanghai, China). Sulfuric acid (H_2SO_4, 98%), H_2O_2 (35%), hydrochloric acid, and ethanol (98%) were brought from Beijing Chemical Reagent Co. (Beijing, China). Sodium fluoride (NaF, >98%), heptahydrate lanthanum chloride ($LaCl_3{\cdot}7H_2O$, 99.9%), heptahydrate cerium chloride ($CeCl_3{\cdot}7H_2O$, 99.9%), oleic acid (90%), 5,5-dimethyl-1-pyrroline *N*-oxide (DMPO), and ascorbic acid (AA) were all purchased from Sigma-Aldrich. Unless otherwise noted, all the chemicals were used without further purification.

Abbreviations: AA, ascorbic acid; LaF_3:Ce NPs, cerium-doped LaF_3 nanoparticles; CL, chemiluminescence; EPR, electron paramagnetic resonance; FT-IR, Fourier transform infrared; PL, photoluminescent; PMT, photomultiplier tube; QDs, quantum dots; RE^{3+}, rare earth ions.

Apparatus

UV-vis absorption spectra were performed on a PerkinElmer Lambda 950 spectrophotometer. The photoluminescent (PL) spectra were collected on an Agilent Cary Eclipse spectrofluorometer. Fourier transform infrared (FT-IR) spectra were obtained on a PerkinElmer Frontier FT-IR spectrometer. CL experiments were conducted with an ultra-weak CL analyzer (IFFM-E, Xi'an Remex Analytical Instrument Co., Ltd, China). Transmission electron microscopy images were obtained on a JEOL-1400 transmission electron microscope (JEOL, Tokyo, Japan). Electron paramagnetic resonance (EPR) spectra were measured on a Bruker E500 spectrometer.

LaF_3:Ce NPs Synthesis

Hydrothermal reaction was utilized to synthesize LaF_3:Ce NPs. 2.25 ml of $LaCl_3$ solution (0.20 M), 1.00 ml of $CeCl_3$ solution (0.05 M), 2.00 ml of NaF solution (1.00 M), 20 ml of ethanol, and 10 ml of oleic acid were mixed and stirred for 0.5 h in reaction kettle. The mixture was heated in an oven and kept at 200°C for 8 h. After reaction, the supernatant was removed. The remnant suspension was centrifuged at 6,000 rpm for 5 min and then the supernatant was also removed. The resultant solid was dispersed in 2.00 M hydrochloric acid. After ethanol addition, the mixture was centrifuged at 6,000 rpm for 5 min to remove the supernatant. The product was stored in 4 ml H_2O for further use. The exact doping percentage of cerium was calculated to be 10%.

CL Study of the LaF_3:Ce NPs-$NaNO_2$-H_2O_2 System

At first, CL intensities of the $NaNO_2$-H_2O_2 system with and without LaF_3:Ce NPs were compared. Fifty microliters of H_2O_2 (3.00 M), which was acidified by 0.04 M H_2SO_4, was injected into the mixture of 50 μl of LaF_3:Ce NPs and 50 μl of $NaNO_2$ (10 μM). In the control experiment, 50 μl of LaF_3:Ce NPs was replaced by 50 μl of H_2O. CL intensities of both the two conditions were recorded and compared. CL profiles were integrated at intervals of 0.1 s. Voltage of the photomultiplier tube (PMT) was set at 1.2 kV. CL spectrum was measured with high-energy cutoff filters (400–640 nm), which were set between the quartz cuvette and PMT as described in Cui et al. (2003). Additional orders of the reagents were investigated to collect CL kinetic curves. EPR measurements were operated at an X-band frequency of 9.85 GHz. Irradiation was performed by using a 300-W Xe lamp (300 nm $< \lambda <$ 1,100 nm) with the output radiation focused on the samples in the cavity by an optical fiber (50 cm length, 0.3 cm diameter). All spectra were acquired at 298 K. DMPO (12.4 μl in 1 ml of H_2O) was taken as the specific detection reagent for ·OH. AA (0.1 mM) was used as a scavenger for $O_2^{\cdot-}$. CL intensities of the LaF_3:Ce NPs-$NaNO_2$-H_2O_2 system with and without AA were recorded.

Nitrite Analysis

Experimental conditions were optimized with different H_2SO_4 concentrations (0, 0.02, 0.03, 0.04, 0.05, and 0.06 M), H_2O_2 concentrations (0.00, 1.00, 2.00, 3.00, 4.00, and 5.00 M), and additional volumes of LaF_3:Ce NPs (0, 10, 20, 30, 40, 50, 60, and 70 μl). The univariate method was adopted in systematically

optimizing experimental parameters through changing one parameter at a time while keeping others constant. At the optimal experimental conditions, calibration curve was recorded by detecting CL intensities vs. different nitrite concentrations.

RESULTS

Characterization of LaF_3:Ce NPs

LaF_3:Ce NPs obtained in this work exhibited hexagonal phase and their average sizes were about 80 × 20 nm (**Figure 1A**). 4*f* shells of lanthanides are partially filled and are effectively shielded by outer 5s and 5p shells leading to satisfactory emissions. The prepared LaF_3:Ce NPs gave a bright blue color under ultraviolet radiation (λ_{ex} = 254 nm) (**Figure 1B**, inset). The emission of LaF_3:Ce NPs shifted to longer wavelength with the increase of excitation wavelength revealing the distribution of different surface energy traps of the LaF_3:Ce NPs (**Figure 1B**). UV-vis absorption spectra of the LaF_3:Ce NPs-$NaNO_2$-H_2O_2 system were collected and are shown in **Figure 1C**. $NaNO_2$ gave an absorption peak at 354 nm, which decreased when acidified H_2O_2 was added. Another absorption peak located at 301 nm appeared due to the isomerization of ONOOH, which was generated in the mixture of acidified H_2O_2 and $NaNO_2$ (Lin et al., 2011), while no new absorption peaks were found when acidified H_2O_2 mixed with LaF_3:Ce NPs. Except the absorption peak of ONOOH, no other new absorption peak was found in the LaF_3:Ce NPs-$NaNO_2$-H_2O_2 system, indicating that no new compound was formed. UV-vis absorption spectra gave some indications for the CL mechanism of this system, which was illustrated in detail in the subsequent section. FT-IR spectrum of LaF_3:Ce NPs indicated that there were O-H groups on the surface of LaF_3:Ce NPs (**Figure 1D**).

CL of the LaF_3:Ce NPs-$NaNO_2$-H_2O_2 System

CL intensities of the $NaNO_2$-H_2O_2 system with and without LaF_3:Ce NPs were sharply different. LaF_3:Ce NPs addition intensely enhanced CL intensity (**Figure 2A**). As shown in **Figure 2B**, the CL spectrum for the LaF_3:Ce NPs-$NaNO_2$-H_2O_2 system was wide ranging from 375 to 500 nm and was centered

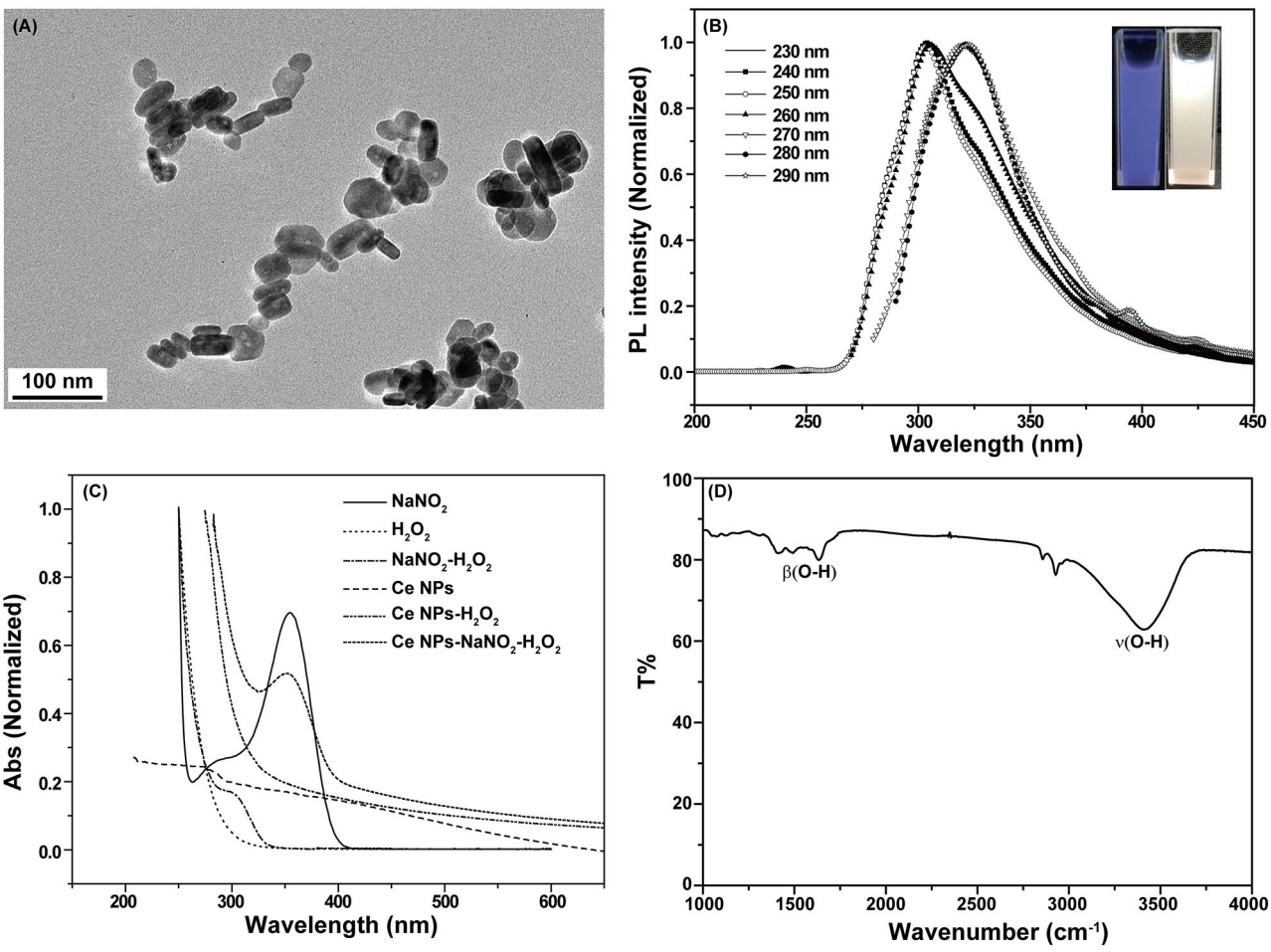

FIGURE 1 | Characterization of LaF_3:Ce NPs. **(A)** Transmission electron microscopy images of LaF_3:Ce NPs. **(B)** PL spectra of LaF_3:Ce NPs. The inset is the photograph of LaF_3:Ce NPs under a UV lamp (λ_{ex} = 254 nm). **(C)** UV-vis absorption spectra of the reagent in the CL reaction. **(D)** FT-IR spectra of LaF_3:Ce NPs.

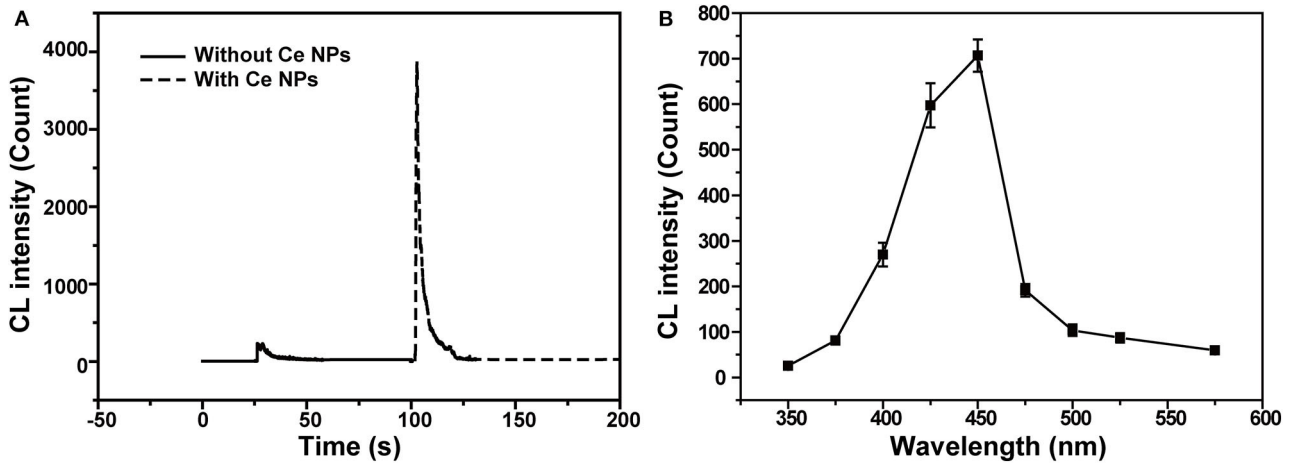

FIGURE 2 | CL profiles of the LaF_3:Ce NPs-$NaNO_2$-H_2O_2 system. **(A)** Comparison of CL intensities of the $NaNO_2$-H_2O_2 system with and without LaF_3:Ce NPs. **(B)** CL spectrum of the LaF_3:Ce NPs-$NaNO_2$-H_2O_2 system. The standard error bars mean the variation of three individual experiments. Conditions: 3.00 M H_2O_2 in 0.04 M H_2SO_4, 50 μl of LaF_3:Ce NPs and 10 μM $NaNO_2$ solution. Voltage of the PMT was set at 1.2 kV.

at 450 nm. The fluorescent emission of LaF_3:Ce NPs is also wide, which is similar to the CL spectrum of the LaF_3:Ce NPs-$NaNO_2$-H_2O_2 system. As a result, it is reasonable to refer that the CL originates from the various surface energy traps existing on the LaF_3:Ce NPs. Compared with the PL peak of LaF_3:Ce NPs, the CL spectrum is red-shifted due to the energy separations of LaF_3:Ce NPs surface states. PL was generated through excitation and emission within the core of the LaF_3:Ce NPs and the energy gap between them is larger than the energy separations on NPs surface (Ding et al., 2002; Myung et al., 2002).

CL Kinetic Study

As described in UV-vis absorption spectra, ONOOH was generated when $NaNO_2$ was mixed with acidified H_2O_2 (Equation 1) (Anbar and Taube, 1954). ONOOH easily transforms to be nitrate via the stage of HOONO* and give emissions during the process (Equation 2) (Houk et al., 1996). The emission locates at 350–450 nm, which overlaps the absorption spectrum of LaF_3:Ce NPs. Hence, LaF_3:Ce NPs can be excited by the energy of transformation and cause CL emission. However, the maximum of the transformation-derived CL was obtained at the pH value of 6.5–7.0 while the maximum CL of the LaF_3:Ce NPs-$NaNO_2$-H_2O_2 system was recorded in a severe acidic solution (Starodubtseva et al., 1999). As a consequence, the transformation energy only partially contributed to the CL of the LaF_3:Ce NPs-$NaNO_2$-H_2O_2 system. Various mixing orders of reagents influenced the reactions between LaF_3:Ce NPs and ONOOH and then affected the CL intensities (**Figure 3A**). The highest CL was obtained when acidified H_2O_2 was injected into the mixture of LaF_3:Ce NPs and $NaNO_2$. At this condition, the generated ONOOH adequately reacted with LaF_3:Ce NPs and gave enhanced CL. Mixing of $NaNO_2$ with acidified H_2O_2 without LaF_3:Ce NPs gave weak and lasting CL while mixing of LaF_3:Ce NPs with acidified H_2O_2 without $NaNO_2$ gave weak and rapid CL (**Figure 3B**).

$$\mathbf{HNO_2 + H_2O_2 \rightarrow ONOOH + H_2O} \quad (1)$$

$$\mathbf{ONOOH \rightarrow ONOOH^* \rightarrow NO_3^- + H^+} \quad (2)$$

CL Mechanism

According to the CL kinetic study, it demonstrated that the reactions between LaF_3:Ce NPs and ONOOH or its related species were the main cause accounting for the enhanced CL. ONOOH was reported to be capable of producing reactive oxygen species (Equations 3–5) (Alvarez et al., 1995; Gunaydin and Houk, 2008; Lin et al., 2011). It was obvious that ONOOH-produced reactive oxygen species include ·OH, $O_2^{\cdot-}$, and $^1O_2$ in this system. EPR was performed and DMPO was utilized as the specific detection reagent for ·OH to directly examine the variation of ·OH after LaF_3:Ce NPs addition. Although CL intensity of the LaF_3:Ce NPs-$NaNO_2$-H_2O_2 system was greatly enhanced, the production of ·OH was almost not increased (**Figure 4A**). $^1O_2$ was derived from ·OH so it could refer that there was no increase in $^1O_2$ quantity. Ethanol was reported to react with ·OH and yield an octet spectrum that was completely distinct from the DMPO-OH spectrum (Finkelstein et al., 1980). The octet spectrum in the LaF_3:Ce NPs-$NaNO_2$-H_2O_2 system rooted in the reaction between ·OH and residual ethanol from treatment process of LaF_3:Ce NPs. Furthermore, AA, which was a scavenger for $O_2^{\cdot-}$, obviously inhibited the CL of the LaF_3:Ce NPs-$NaNO_2$-H_2O_2 system (**Figure 4B**). All the results indicated that $O_2^{\cdot-}$ was the critical reason for the enhanced CL instead of ·OH and $^1O_2$. $O_2^{\cdot-}$ acting as an electron donor reacted with LaF_3:Ce NPs to produce LaF_3:Ce $NPs^{\cdot-}$ (Equation 6) (Poznyak et al., 2004). ONOOH serving as a hole injector converted LaF_3:Ce NPs to LaF_3:Ce $NPs^{\cdot+}$ (Equation 7). Electron–hole annihilation between LaF_3:Ce $NPs^{\cdot-}$ and LaF_3:Ce $NPs^{\cdot+}$ resulted in CL emission (Equation 8) (**Figure 5**; Ding et al., 2002;

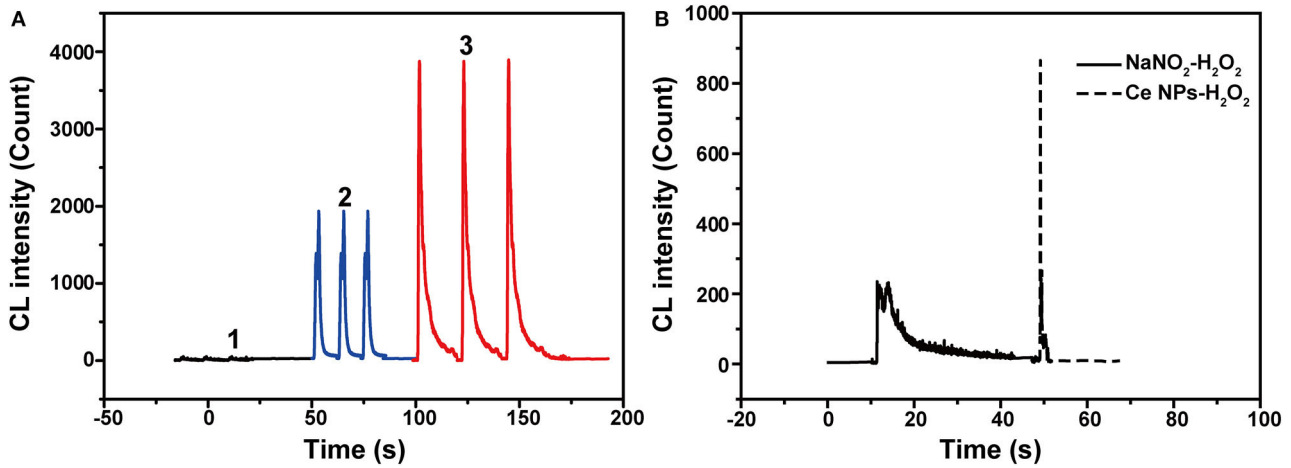

FIGURE 3 | CL kinetic study of the LaF_3:Ce NPs-$NaNO_2$-H_2O_2 system. **(A)** CL kinetic curves of the LaF_3:Ce NPs-$NaNO_2$-H_2O_2 system with different reagent mixing orders: **1**. injecting LaF_3:Ce NPs into the mixture of $NaNO_2$ and acidified H_2O_2; **2**. injecting $NaNO_2$ into the mixture of LaF_3:Ce NPs and acidified H_2O_2; **3**. injecting acidified H_2O_2 into the mixture of LaF_3:Ce NPs and $NaNO_2$. CL signals of three repeated experiments were given. **(B)** CL kinetic curves of the $NaNO_2$-H_2O_2 system and the LaF_3:Ce NPs-H_2O_2 system. Conditions: 3.00 M H_2O_2 in 0.04 M H_2SO_4, 50 μl of LaF_3:Ce NPs and 10 μM $NaNO_2$ solution. Voltage of the PMT was set at 1.2 kV.

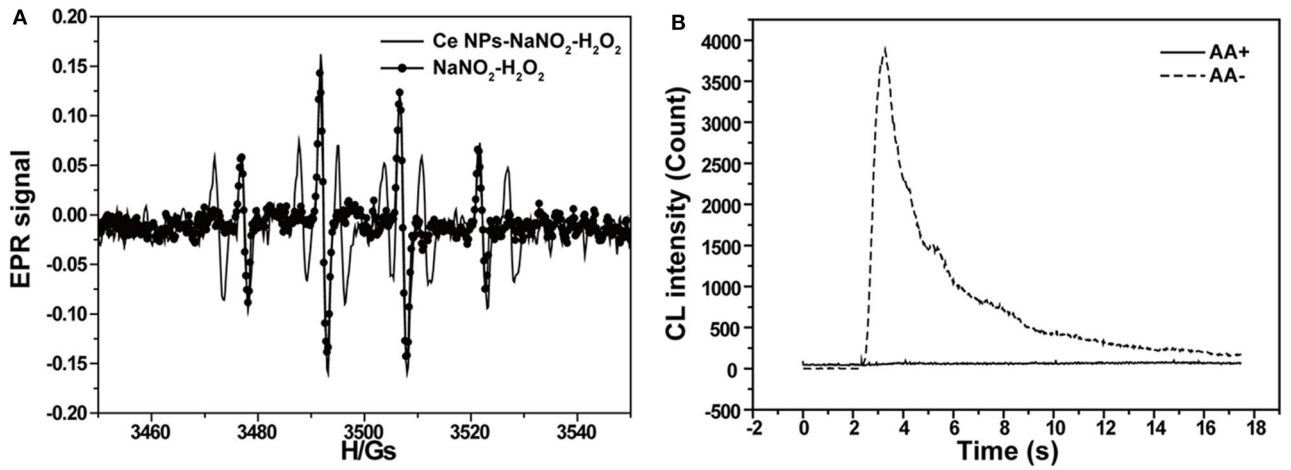

FIGURE 4 | CL mechanism study of the LaF_3:Ce NPs-$NaNO_2$-H_2O_2 system. **(A)** EPR spectra of ·OH generated via the reaction of DMPO probe in the LaF_3:Ce NPs-$NaNO_2$-H_2O_2 and $NaNO_2$-H_2O_2 systems. **(B)** CL profiles of the LaF_3:Ce NPs-$NaNO_2$-H_2O_2 system with and without AA. Conditions: 3.00 M H_2O_2 in 0.04 M H_2SO_4, 50 μl of LaF_3:Ce NPs, 10 μM $NaNO_2$ solution, 12.4 μl of DMPO in 1 ml of H_2O, and 0.1 mM AA. Voltage of the PMT was set at 1.2 kV.

Poznyak et al., 2004; Zheng et al., 2009; Dong et al., 2010).

$$ONOOH \rightarrow \cdot NO_2 + \cdot OH \quad (3)$$

$$ONOOH + H_2O_2 \rightarrow O_2^{\cdot -} + \cdot NO_2 + H^+ + H_2O \quad (4)$$

$$O_2^{\cdot -} + \cdot OH \rightarrow {}^1O_2 + OH^- \quad (5)$$

$$LaF_3{:}Ce\ NPs + O_2^{\cdot -} \rightarrow LaF_3{:}Ce\ NPs^{\cdot -} + O_2 \quad (6)$$

$$LaF_3{:}Ce\ NPs + ONOOH \rightarrow LaF_3{:}Ce\ NPs^{\cdot +} + \cdot NO_2 + H_2O \quad (7)$$

$$LaF_3{:}Ce\ NPs^{\cdot +} + LaF_3{:}Ce\ NPs^{\cdot -} \rightarrow LaF_3{:}Ce\ NPs^* + LaF_3{:}Ce\ NPs \rightarrow 2LaF_3{:}Ce\ NPs + hv \quad (8)$$

Nitrite Analysis

To establish the optimal conditions for nitrite analysis, the volume of LaF_3:Ce NPs added into the CL system and concentrations of H_2SO_4 and H_2O_2 were investigated, respectively. As shown in **Figure 6A**, 50 μl of LaF_3:Ce NPs was added into the CL system and provided the highest CL emission. Less LaF_3:Ce NPs inadequately reacted with ONOOH while surplus LaF_3:Ce NPs also consumed energy. Reactive substance ONOOH was the product of $NaNO_2$ and H_2O_2 in acid medium, so H_2SO_4 was indispensable for the CL system. No CL signals could be observed in the absence of H_2SO_4. The most intense

CL signal was obtained with the H_2SO_4 concentration of 0.04 M (**Figure 6B**). CL signal increased with the concentration of H_2O_2 in the range from 0 to 3.00 M (**Figure 6C**). Hence, the optimal analytical conditions for nitrite analysis were 3.00 M H_2O_2 in 0.04 M H_2SO_4 injected into the mixture of 50 μl of LaF_3:Ce NPs and nitrite solution.

Under the optimal conditions, CL signals for different nitrite concentrations were recorded and shown in **Figure 7**. Good linear relationship between CL intensity and nitrite concentration was obtained in the range from 1 to 100 μM with a correlation coefficient of 0.9981 ($y = 256.3x + 42.72$). The relative standard deviation values of the analysis were 8.7, 1.2, and 4.8% for nitrite concentrations of 1, 10, and 100 μM, respectively. Relative standard deviation values demonstrated the satisfactory reproducibility. The limit of detection ($S/N = 3$) for nitrite was 0.33 μM.

DISCUSSION

The eternal goals and challenges of analytical chemistry are developing accurate, automated, selective, stable, sensitive, high-speed, high-throughput, and *in situ* analytical methods and protocols (Ju, 2013). The combination of analytical chemistry with new materials, especially nanomaterials, is the current frontier research topics and exhibits greatly improved analytical capacities. CL analysis is a traditional analytical technology and possesses outstanding advantages, such as low cost, simple instrument, fast response, and high compatibility. The application of nanomaterials in CL analysis leads to new CL sensing disciplines and offers a broad palette of opportunities for analytical chemists. In 2004, Poznyak et al. (2004) firstly reported the nanocrystal band gap CL derived from CdSe/CdS core-shell QDs that acted as a novel class of luminophores with the emission state originated from quantum-confined orbitals. Superior emission properties in QDs gave promises for developing QD-based nanoprobes for CL analysis. Besides traditional semiconductor QDs, some novel nanomaterials, such as carbon nanodots (Lin et al., 2011), graphene QDs (Hassanzadeh and Khataee, 2018), graphitic carbon nitride QDs (Zhu et al., 2019), and N-dots (Zheng et al., 2017), were developed to be potential platforms for CL

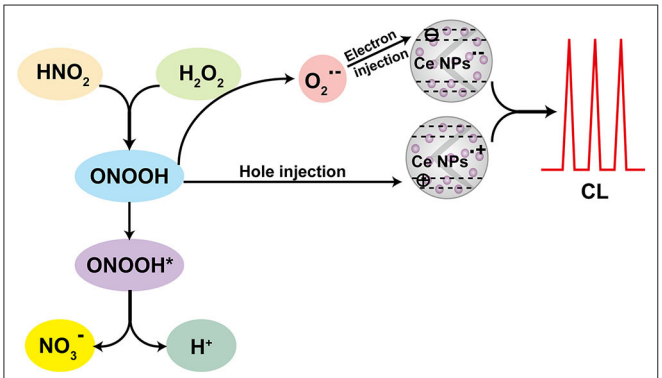

FIGURE 5 | Schematic illustration of the CL mechanism of the LaF_3:Ce NPs-$NaNO_2$-H_2O_2 system.

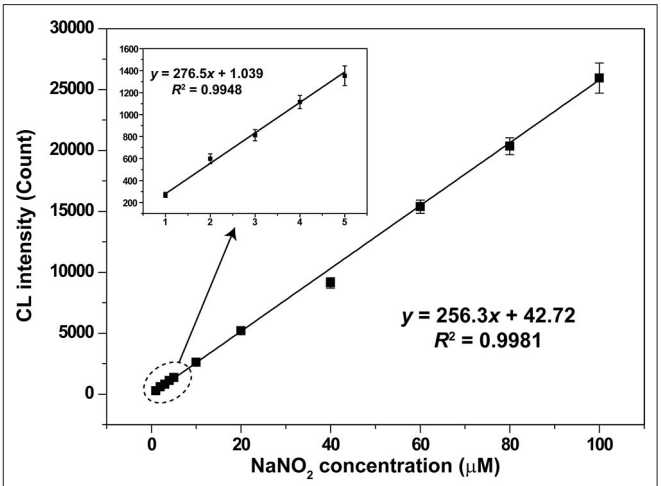

FIGURE 7 | Calibration curve for nitrite analysis based on the LaF_3:Ce NPs-enhanced CL. The standard error bars mean the variation of three individual experiments. Conditions: 3.00 M H_2O_2 in 0.04 M H_2SO_4 and 50 μl of LaF_3:Ce NPs. Voltage of the PMT was set at 1.2 kV.

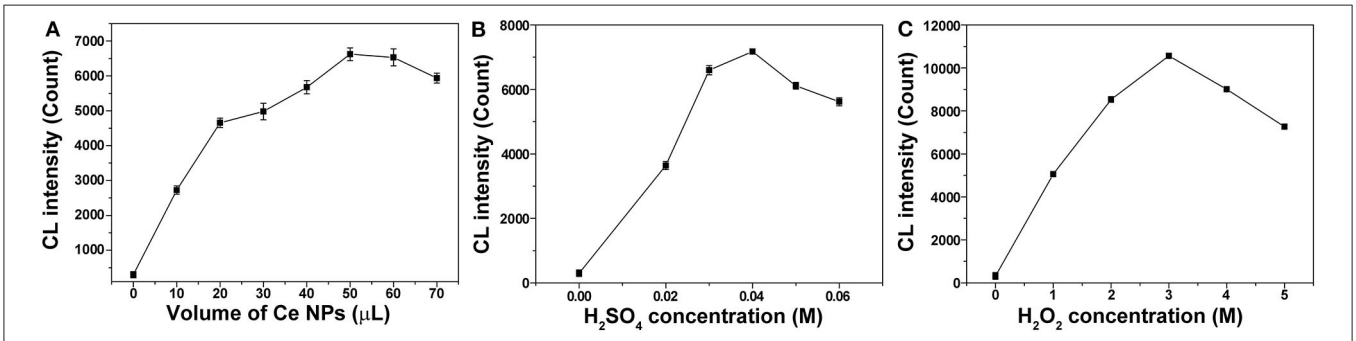

FIGURE 6 | Optimization of experimental conditions for nitrite analysis. **(A)** Volume of LaF_3:Ce NPs added into the CL system was optimized. **(B)** Concentration of H_2SO_4 used to acidify H_2O_2 was optimized. **(C)** Concentration of H_2O_2 was optimized. The standard error bars mean the variation of three individual experiments.

sensing. These nanomaterials are superior in terms of robust chemical inertness, low toxicity, good aqueous solubility, high resistance to photobleaching, and satisfactory biocompatibility. Our work is an endeavor step during the development process of nanomaterial-sensitized CL analysis methods. In this study, LaF_3:Ce NPs were successfully synthesized and applied in nitrite detection based on CL signals. The synthetic process of LaF_3:Ce NPs was simple and the products were fully characterized to give indications for the CL mechanism study. The enhancement of LaF_3:Ce NPs for the $NaNO_2$-H_2O_2 CL system was efficient and the mechanism was systematically and scientifically explained. The linear relationship between CL intensity and nitrite concentration was found, although there were spaces for improving the limit of detection. This work tried to explore new CL nanoprobes and gave a new route for fluoride applications. In the future, there is still a great demand for developing novel CL nanoprobes especially metal-free QDs and two-dimensional QDs.

CONCLUSIONS

In summary, LaF_3:Ce NPs were successfully synthesized and demonstrated to intensely enhance ultra-weak CL of the $NaNO_2$-H_2O_2 system. The CL mechanism was suggested to be the electron–hole annihilation between hole-injected and electron-injected LaF_3:Ce NPs. The new CL system was developed to be a novel, simple, and straightforward analytical method for nitrite. All the experimental conditions were optimized and a satisfactory linear relationship between CL intensity and nitrite concentration was obtained. This work shed a new light on the research and application of traditional fluoride NPs doped with RE^{3+}.

DATA AVAILABILITY STATEMENT

The raw data supporting the conclusions of this article will be made available by the authors, without undue reservation, to any qualified researcher.

AUTHOR CONTRIBUTIONS

YuW organized and conducted all the experiments, analyzed data, and wrote the manuscript. JW coordinated the project, supervised all the experiments, analyzed data, and wrote, edited, and reviewed the manuscript. YaW assisted the experiments of nitrite analysis. CH synthesized and characterized LaF_3:Ce NPs. TC performed experiments of the CL study of the LaF_3:Ce NPs-$NaNO_2$-H_2O_2 system. All authors contributed to the article and approved the submitted version.

FUNDING

This work was supported by the National Natural Science Foundation of China (No. 21874120) and the Fundamental Research Funds for the Central Universities (No. 2652018004). During the revision process, support was supplied by the Fundamental Research Funds for the Central Universities (No. 2652019112) and the open fund of Key Laboratory of Optic-electric Sensing and Analytical Chemistry for Life Science, MOE, Qingdao University of Science and Technology (No. OESACLS202004).

ACKNOWLEDGMENTS

Ms. Mengnan Rao is acknowledged for conducting some preparation works.

REFERENCES

All, A. H., Zeng, X., Teh, D. B. L., Yi, Z., Prasad, A., and Ishizuka, T., et al. (2019). Expanding the toolbox of upconversion nanoparticles for *in vivo* optogenetics and neuromodulation. *Adv. Mater.* 31:1803474. doi: 10.1002/adma.201803474

Alvarez, B., Denicola, A., and Radi, R. (1995). Reaction between peroxynitrite and hydrogen peroxide: formation of oxygen and slowing of peroxynitrite decomposition. *Chem. Res. Toxicol.* 8, 859–864. doi: 10.1021/tx00048a006

Anbar, M., and Taube, H. (1954). Interaction of nitrous acid with hydrogen peroxide and with water. *J. Am. Chem. Soc.* 76, 6243–6247. doi: 10.1021/ja01653a007

Bekah, D., Cooper, D., Kudinov, K., Hill, C., Seuntjens, J., and Bradforth, S., et al. (2016). Synthesis and characterization of biologically stable, doped LaF_3 nanoparticles co-conjugated to PEG and photosensitizers. *J. Photochem. Photobiol. A Chem.* 329, 26–34. doi: 10.1016/j.jphotochem.2016.06.008

Bender, C. M., Burlitch, J. M., Barber, D., and Pollock, C. (2000). Synthesis and fluorescence of neodymium-doped barium fluoride nanoparticles. *Chem. Mater.* 12, 1969–1976. doi: 10.1021/cm9904741

Cao, R., Huang, H., Liang, J., Wang, T., Luo, Y., and Asiri, A. M., et al. (2019). A MoN nanosheet array supported on carbon cloth as an efficient electrochemical sensor for nitrite detection. *Analyst* 144, 5378–5380. doi: 10.1039/C9AN01270B

Cui, H., Zou, G., and Lin, X. (2003). Electrochemiluminescence of luminol in alkaline solution at a paraffin-impregnated graphite electrode. *Anal. Chem.* 75, 324–331. doi: 10.1021/ac0201631

Dai, C., Wang, J., Fu, Y., Zhou, H., and Song, Q. (2017). Selective and real-time detection of nitric oxide by a two-photon fluorescent probe in live cells and tissue slices. *Anal. Chem.* 89, 10511–10519. doi: 10.1021/acs.analchem.7b02680

Ding, Z., Quinn, B. M., Haram, S. K., Pell, L. E., Korgel, B. A., and Bard, A. J. (2002). Electrochemistry and electrogenerated chemiluminescence from silicon nanocrystal quantum dots. *Science* 296, 1293–1297. doi: 10.1126/science.1069336

Dong, Y., Zhou, N., Lin, X., Lin, J., Chi, Y., and Chen, G. (2010). Extraction of electrochemiluminescent oxidized carbon quantum dots from activated carbon. *Chem Mater.* 22, 5895–5899. doi: 10.1021/cm1018844

Dou, X., Zhang, Q., Shah, S. N. A., Khan, M., Uchiyama, K., and Lin, J. (2019). MoS_2-quantum dot triggered reactive oxygen species generation and depletion, responsible for enhanced chemiluminescence. *Chem. Sci.* 10, 497–500. doi: 10.1039/C8SC03511C

Finkelstein, E., Rosen, G. M., and Rauckman, E. J. (1980). Spin trapping kinetics of the reaction of superoxide and hydroxyl radicals with nitrones. *J. Am. Chem. Soc.* 102, 4994–4999. doi: 10.1021/ja00535a029

Gunaydin, H., and Houk, K. N. (2008). Molecular dynamics simulation of the HOONO decomposition and the HO•/NO_2• caged radical pair in water. *J. Am. Chem. Soc.* 130, 10036–10037. doi: 10.1021/ja711365e

Han, S., Samanta, A., Xie, X., Huang, L., Peng, J., and Park, S. J., et al. (2017). Gold and hairpin DNA functionalization of upconversion nanocrystals for imaging and *in vivo* drug delivery. *Adv. Mater.* 29:1700244. doi: 10.1002/adma.201700244

Hassanzadeh, J., and Khataee, A. (2018). Ultrasensitive chemiluminescent biosensor for the detection of cholesterol based on synergetic peroxidase-like activity of MoS_2 and graphene quantum dots. *Talanta* 178, 992–1000. doi: 10.1016/j.talanta.2017.08.107

Houk, K. N., Condroski, K. R., and Pryor, W. A. (1996). Radical and concerted mechanisms in oxidations of amines, sulfides, and alkenes by peroxynitrite, peroxynitrous acid, and the peroxynitrite–CO_2 adduct: density functional theory transition structures and energetics. *J. Am. Chem. Soc.* 118, 13002–13006. doi: 10.1021/ja9619521

Hu, Y., Wu, B., Jin, Q., Wang, X., Li, Y., and Sun, Y., et al. (2016). Facile synthesis of 5 nm $NaYF_4$:Yb/Er nanoparticles for targeted upconversion imaging of cancer cells. *Talanta* 152, 504–512. doi: 10.1016/j.talanta.2016.02.039

Jana, J., Lee, H. J., Chung, J. S., Kim, M. H., and Hur, S. H. (2019). Blue emitting nitrogen-doped carbon dots as a fluorescent probe for nitrite ion sensing and cell-imaging. *Anal. Chim. Acta* 1079, 212–219. doi: 10.1016/j.aca.2019.06.064

Ju, H. (2013). Grand challenges in analytical chemistry, towards more bright eyes for scientific research, social events and human health. *Front. Chem.* 1:5. doi: 10.3389/fchem.2013.00005

Ju, J., Won, H., Jung, J., Yeo, J., Van Cuong, P., and Kim, D. (2017). Enhanced X-ray excited luminescence of LaF_3:Ce/CdSeS nanocomposites by resonance energy transfer for radiation detection. *J. Electron. Mater.* 46, 5319–5323. doi: 10.1007/s11664-017-5548-z

Li, S., Zhang, X., Hou, Z., Cheng, Z., Ma, P., and Lin, J. (2012). Enhanced emission of ultra-small-sized LaF_3:RE^{3+} (RE = Eu, Tb) nanoparticles through 1,2,4,5-benzenetetracarboxylic acid sensitization. *Nanoscale* 4, 5619–5626. doi: 10.1039/c2nr31206a

Lin, Z., Xue, W., Chen, H., and Lin, J. (2011). Peroxynitrous-acid-induced chemiluminescence of fluorescent carbon dots for nitrite sensing. *Anal. Chem.* 83, 8245–8251. doi: 10.1021/ac202039h

Lu, C., Lin, J., Huie, C. W., and Yamada, M. (2004). Chemiluminescence study of carbonate and peroxynitrous acid and its application to the direct determination of nitrite based on solid surface enhancement. *Anal. Chim. Acta* 510, 29–34. doi: 10.1016/j.aca.2003.12.057

Lu, C., Qu, F., Lin, J., and Yamada, M. (2002). Flow-injection chemiluminescent determination of nitrite in water based on the formation of peroxynitrite from the reaction of nitrite and hydrogen peroxide. *Anal. Chim. Acta* 474, 107–114. doi: 10.1016/S0003-2670(02)01010-3

Ma, Y., Wang, Y., Xie, D., Gu, Y., Zhang, H., and Wang, G., et al. (2018). NiFe-Layered double hydroxide nanosheet arrays supported on carbon cloth for highly sensitive detection of nitrite. *ACS Appl. Mater. Inter.* 10, 6541–6551. doi: 10.1021/acsami.7b16536

Madhuvilakku, R., Alagar, S., Mariappan, R., and Piraman, S. (2020). Glassy carbon electrodes modified with reduced graphene oxide-MoS_2-poly (3, 4-ethylene dioxythiophene) nanocomposites for the non-enzymatic detection of nitrite in water and milk. *Anal. Chim. Acta* 1093, 93–105. doi: 10.1016/j.aca.2019.09.043

Myung, N., Ding, Z., and Bard, A. J. (2002). Electrogenerated chemiluminescence of CdSe nanocrystals. *Nano Lett.* 2, 1315–1319. doi: 10.1021/nl0257824

Nampoothiri, P. K., Gandhi, M. N., and Kulkarni, A. R. (2017). Elucidating the stabilizing effect of oleic acid coated LaF_3: Nd^{3+} nanoparticle surface in the thermal degradation of PMMA nanocomposites. *Mater. Chem. Phys.* 190, 45–52. doi: 10.1016/j.matchemphys.2016.12.075

Pires, N. M. M., Dong, T., and Yang, Z. (2019). A fluorimetric nitrite biosensor with polythienothiophene-fullerene thin film detectors for on-site water monitoring. *Analyst* 144, 4342–4350. doi: 10.1039/C8AN02441C

Poznyak, S. K., Talapin, D. V., Shevchenko, E. V., and Weller, H. (2004). Quantum dot chemiluminescence. *Nano Lett.* 4, 693–698. doi: 10.1021/nl049713w

Schuyt, J. J., and Williams, G. V. M. (2018). Photoluminescence, radioluminescence and optically stimulated luminescence in nanoparticle and bulk $KMgF_3$(Eu). *J. Lumin.* 204, 472–479. doi: 10.1016/j.jlumin.2018.08.056

Starodubtseva, M. N., Cherenkevich, S. N., and Semenkova, G. N. (1999). Investigation of the interaction of sodium nitrite with hydrogen peroxide in aqueous solutions by the chemiluminescence method. *J. Appl. Spectrosc.* 66, 473–476. doi: 10.1007/BF02676785

Vijayan, A. N., Liu, Z., Zhao, H., and Zhang, P. (2019). Nicking enzyme-assisted signal-amplifiable Hg^{2+} detection using upconversion nanoparticles. *Anal. Chim. Acta* 1072, 75–80. doi: 10.1016/j.aca.2019.05.001

Wang, Q., Yu, L., Liu, Y., Lin, L., Lu, R., and Zhu, J., et al. (2017). Methods for the detection and determination of nitrite and nitrate: A review. *Talanta* 165, 709–720. doi: 10.1016/j.talanta.2016.12.044

Wang, R., Wang, Z., Xiang, X., Zhang, R., Shi, X., and Sun, X. (2018). MnO_2 nanoarrays: an efficient catalyst electrode for nitrite electroreduction toward sensing and NH_3 synthesis applications. *Chem. Commun.* 54, 10340–10342. doi: 10.1039/C8CC05837G

Wu, J., Wang, X., Lin, Y., Zheng, Y., and Lin, J. (2016). Peroxynitrous-acid-induced chemiluminescence detection of nitrite based on Microfluidic chip. *Talanta* 154, 73–79. doi: 10.1016/j.talanta.2016.03.062

Wu, J., Yang, Z., Qiu, C., Zhang, Y., Wu, Z., and Yang, J., et al. (2018). Enhanced performance of a graphene/GaAs self-driven near-infrared photodetector with upconversion nanoparticles. *Nanoscale* 10, 8023–8030. doi: 10.1039/C8NR00594J

Wu, N., Gu, Y., Kong, M., Liu, Q., Cheng, S., and Yang, Y., et al. (2020). Yb-based nanoparticles with the same excitation and emission wavelength for sensitive *in vivo* biodetection. *Anal. Chem.* 92, 2027–2033. doi: 10.1021/acs.analchem.9b04448

Wu, Y., Xu, J., Poh, E. T., Liang, L., Liu, H., and Yang, J. K. W., et al. (2019). Upconversion superburst with sub-2 μs lifetime. *Nat. Nanotechnol.* 14, 1110–1115. doi: 10.1038/s41565-019-0560-5

Yan, S., Zeng, X., Tang, Y., Liu, B., Wang, Y., and Liu, X. (2019). Activating antitumor immunity and antimetastatic effect through polydopamine-encapsulated core-shell upconversion nanoparticles. *Adv. Mater.* 31:1905825. doi: 10.1002/adma.201905825

Yi, Z., Luo, Z., Barth, N. D., Meng, X., Liu, H., and Bu, W., et al. (2019). *In vivo* tumor visualization through MRI Off-On switching of $NaGdF_4$-$CaCO_3$ nanoconjugates. *Adv. Mater.* 31, 1901851. doi: 10.1002/adma.201901851

Zeng, X., Chen, S., Weitemier, A., Han, S., Blasiak, A., and Prasad, A., et al. (2019). Visualization of intra-neuronal motor protein transport through upconversion microscopy. *Angew. Chem. Int. Edit.* 58, 9262–9268. doi: 10.1002/anie.201904208

Zhang, L., Wu, X., Yuan, Z., and Lu, C. (2018). Π-Conjugated thiolate amplified spectrophotometry nitrite assay with improved sensitivity and accuracy. *Chem. Commun.* 54, 12178–12181. doi: 10.1039/C8CC06477F

Zhang, Y., Nie, J., Wei, H., Xu, H., Wang, Q., and Cong, Y., et al. (2018). Electrochemical detection of nitrite ions using Ag/Cu/MWNT nanoclusters electrodeposited on a glassy carbon electrode. *Sens. Actuator B Chem.* 258, 1107–1116. doi: 10.1016/j.snb.2017.12.001

Zheng, H., Guan, X., Mao, X., Zhu, Z., Yang, C., and Qiu, H., et al. (2018). Determination of nitrite in water samples using atmospheric pressure glow discharge microplasma emission and chemical vapor generation of NO species. *Anal. Chim. Acta* 1001, 100–105. doi: 10.1016/j.aca.2017.11.060

Zheng, L., Chi, Y., Dong, Y., Lin, J., and Wang, B. (2009). Electrochemiluminescence of water-soluble carbon nanocrystals released electrochemically from graphite. *J. Am. Chem. Soc.* 131, 4564–4565. doi: 10.1021/ja809073f

Zheng, Y., Zhang, D., Shah, S. N. A., Li, H., and Lin, J. (2017). Ultra-weak chemiluminescence enhanced by facilely synthesized nitrogen-rich quantum dots through chemiluminescence resonance energy transfer and electron hole injection. *Chem. Commun.* 53, 5657–5660. doi: 10.1039/C7CC02041D

Zhou, Y., Ma, M., He, H., Cai, Z., Gao, N., and He, C., et al. (2019). Highly sensitive nitrite sensor based on AuNPs/RGO nanocomposites modified graphene electrochemical transistors. *Biosens. Bioelectron.* 146, 111751. doi: 10.1016/j.bios.2019.111751

Zhu, R., Zhang, Y., Fang, X., Cui, X., Wang, J., and Yue, C., et al. (2019). *In situ* sulfur-doped graphitic carbon nitride nanosheets with

enhanced electrogenerated chemiluminescence used for sensitive and selective sensing of l-cysteine. *J. Mater. Chem. B.* 7, 2320–2329. doi: 10.1039/C9TB00301K

Conflict of Interest: The authors declare that the research was conducted in the absence of any commercial or financial relationships that could be construed as a potential conflict of interest.